Effect of Nose Geometry on the Aerothermodynamic Environment of Shuttle Entry Configurations

JOHN J. BERTIN* AND H. TOM FARIA†
The University of Texas at Austin, Austin, Texas
WINSTON D. GOODRICH‡
NASA Johnson Space Center, Houston, Texas
AND
W. R. MARTINDALE§
ARO Inc., Arnold Air Force Station, Tenn.

Surface-pressure data, heat-transfer data, oil-flow patterns, and schlierens have been obtained for two shuttle entry-configurations. Wind-tunnel data were obtained for freestream Mach numbers of 5 and 8 with freestream Reynolds numbers based on model length of 1.5×10^6 to 1.3×10^7 for alphas from 20° to 50°. Transition locations determined using the heating distribution for the windward pitch-plane indicate that cross flow significantly increases the value of $(Re_\theta/M_e)_{tr}$ but that the relatively abrupt cross-sectional change at the wing:fuselage junction trips the boundary layer. Only on the canopy's forward-facing surface did the leeward heating approach the windward values. The presence of the canopy caused the heating to the leeward fuselage to be uniformly low by breaking up the strong axial flow and inducing another separation.

Nomenclature

h	= local heat-transfer coefficient
$h_{t,R=0.3m}$	= calculated heat-transfer coefficient for the stagnation point of a 0.3 m radius sphere scaled to model size
L	= total length of orbiter model, measured along the fuselage axis
M	= Mach number
p	= local static pressure
p_{t2}	= stagnation pressure behind a normal shock
Re_θ	= Reynolds number based on local flow properties and the momentum thickness (evaluated at transition location)
$Re_{\infty,L}$	= freestream Reynolds number based on model length
x	= distance along orbiter axis
α	= angle of attack (alpha)

Subscripts

e	= properties evaluated at the edge of the boundary layer
pk	= peak value
∞	= freestream value

Introduction

IN order to predict the convective heat-transfer distribution for the nose/canopy region of the space-shuttle entry-configuration (i.e., the orbiter), one must describe the three-dimensional flowfield, which may include extensive regions of separated flow. Because of the complexity of the flowfield for the nose/canopy region, experimental data are needed to define the relation between the nose geometry and the resultant flowfield. Although solutions for the laminar, compressible three-dimensional boundary layer have been obtained[1] in conjunction with approximate inviscid windward surface flowfields, the method is very complex. However, procedures of sufficient accuracy for engineering correlations have been developed which can be used to generate theoretical heat-transfer-rate distributions for the windward pitch-plane.[2]

For leeward side flows, two basic separation concepts have been identified by Wang[3]: a bubble-type separation and a free-vortex layer. Wang studied three-dimensional separation-patterns using solutions of the incompressible, laminar boundary-layer near the symmetry plane of an inclined prolate-spheroid. Whereas two-dimensional boundary-layer separation corresponds to the vanishing of skin friction, it is not necessary that the two components of skin friction vanish for three-dimensional separation.

Surface-pressure measurements, oil-flow patterns, and pitot-pressure surveys[4] indicate a free-vortex-layer type of separation for hypersonic flow past a blunt cone at alphas between 6° and 18°. The oil-flow patterns indicated that the circumferential component of the flow which was initially directed toward the leeward plane of symmetry reversed direction. Two symmetrical separation lines developed downstream of the region where the circumferential component of skin friction passed through zero. At the separation line, the oil accumulated and traveled down the separation line to the rear of the cone. Since the oil near the leeward plane of symmetry continued to flow from the attached region through the region of zero lateral skin friction and into the vortex region, the longitudinal component of skin friction was always finite. This flow-separation model contains symmetrical, supersonic, helical vortices close to the surface with an attachment line on the most leeward ray.

Although these separation patterns were obtained for simple shapes, they contain features common to the more complex separated regions of the shuttle orbiter. The leeward flowfield of the orbiter is dependent on configuration geometry, on the angle of attack, and on the flow conditions. The flow mechanism

Submitted July 11, 1973; presented as Paper 73-638 at the AIAA 6th Fluid and Plasma Dynamics Conference, Palm Springs, Calif., July 16–18, 1973; revision received December 18, 1973. This work was supported by the NASA Johnson Space Center, Contract NAS 9-10976.

Index categories: Boundary Layers and Convective Heat Transfer—Laminar; Boundary Layers and Convective Heat Transfer—Turbulent; Jets, Wakes, and Viscid-Inviscid Flow Interactions.

* Associate Professor, Department of Aerospace Engineering and Engineering Mechanics. Member AIAA.

† Research Assistant, Department of Aerospace Engineering and Engineering Mechanics. Member AIAA.

‡ Aerospace Technologist. Member AIAA.

§ Project Engineer. Member AIAA.

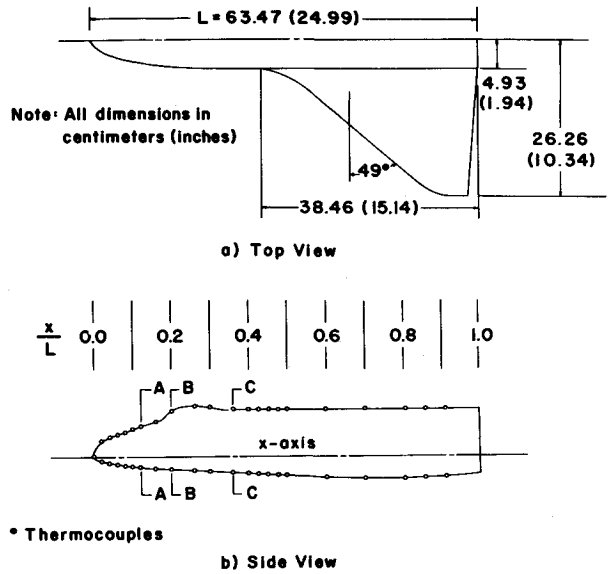

Fig. 1 A sketch of models used in Tunnel B(AEDC) test program.

of greatest importance to the surface environment in the separated region is the free-vortex layer. Reattachment of the vortical flow results in high heating rates to the leeward surface, with local heat-transfer coefficients often exceeding the zero angle-of-attack values. Relatively high leeward-heating has been experimentally observed by Hefner and Whitehead[5,6] for space-shuttle orbiter configurations. Hefner and Whitehead also found that the heat transfer to the lee surface of orbiter-like noses could be reduced by modifying the upper-surface geometry to induce vortex lift-off. The side-view geometry was modified by increasing the initial slope of the lee meridian and then breaking it sharply, which reduced the heating level significantly along 50% of the leeward meridian.

The present investigation studied the effect of nose geometry on the transition criteria for the windward boundary layer, on the extent of separation, on the heat-transfer perturbation due to the canopy, and on the surface pressure and the heat transfer in the separated region. Surface-pressure data, heat-transfer data, oil-flow patterns, and schlieren (or shadowgraph) photographs were obtained for two orbiter configurations. Data were obtained in AEDC Tunnel B and in the University's Supersonic Wind Tunnel (UT SWT) for freestream Mach numbers of 5 and 8 with freestream Reynolds numbers based on model length of 1.5×10^6 to 1.3×10^7.

Experimental Program

Two configurations (referred to herein as the UTN2 and the UTN7) were studied in the present program. The UTN2 had a relatively blunt planform (i.e., a 5:2 ellipse), a relatively flat windward surface, and a leeward geometry which was intended to fix boundary-layer separation. The UTN7 configuration had a more slender planform (i.e., a 4:1 ellipse) and elliptic cross sections. Figures 1 and 2 illustrate the geometry of the two configurations.

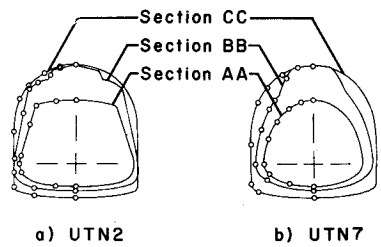

Fig. 2 Sketch of selected cross sections illustrating the two nose configurations.

The model design philosophy was to generate nose configurations whose surface geometry could be described by analytic functions. Furthermore, both the transverse and the longitudinal radii of curvature of the functions defining the windward keel were to be continuous, since the shear layers associated with inflections in the bow shock wave have been found to promote boundary-layer transition.[7] Aft of the station where the wing-root fairing intersected the fuselage ($x = 0.4L$), the configurations were identical. Because the windward surface of the fuselage was flat, a fairing was required to join the rounded windward surface of the nose with the flat-bottomed fuselage. The magnitude of the wing-root fairing, or fillet, is indicated in Fig. 2 by the change required in the cross sections to achieve a flat windward surface at $x = 0.4L$. The complex concave surface which was formed by this wing-root fairing in the region from $x = 0.3L$ to $x = 0.4L$ had a marked effect on the windward flowfield, as will be discussed later.

The two 0.019 scale models (refer to the dimensions in Fig. 1) used in AEDC Tunnel B were constructed of electroformed nickel deposited on a male mandrel. Thus, there was no nose: fuselage junction on the windward surface, which would promote boundary-layer transition. The thin nickel skin was instrumented with 30-gage chromel-alumel thermocouples. For the tests in the UT SWT, 0.0047 scale models of the UTN2 and the UTN7 were built of plastic casting resins. Because of the limited size of the test-section, the University models were not only of smaller scale but represented only the nose region of the two orbiter configurations. Detailed information about the configuration geometries and the models is available in Ref. 8.

Heat-transfer distributions, oil-flow patterns, and shadowgraphs were obtained in Tunnel B at a freestream Mach number of 8 over a range of freestream Reynolds numbers based on model length from 1.5×10^6 to 8×10^6. Surface-pressure distributions, oil-flow patterns, and schlieren photographs were obtained in the UT SWT at a freestream Mach number of 5. The length Reynolds number for the UT tests based on the model length, which would exist if the entire configuration were simulated, varied from 8×10^6 to 13×10^6. The nominal test schedules are presented in Table 1. Although there are exceptions, data were usually obtained for both geometries at a given condition. For the UT SWT program, the highest angle of attack was more nearly 40° for the UTN7 and 45° for the UTN2.

Table 1 Nominal test schedules

a) UT SWT

$Re_{\infty,L}$ \ α	20°	25°	30°	35°	40°	50°
8×10^6	x	x	x	...	x	...
9.5×10^6	x	x	x	...	x	...
13×10^6	x	x	x	...	x	...

b) Tunnel B of AEDC

$Re_{\infty,L}$ \ α	20°	25°	30°	35°	40°	50°
1.6×10^6	x	...	x	x	x	x
3×10^6	...	...	x	...	...	...
4×10^6	x	x	x	x	x	x
6×10^6	...	...	x	...	...	...
7×10^6	x	...	x	...	...	...
8×10^6	x	...	x	...	x	x

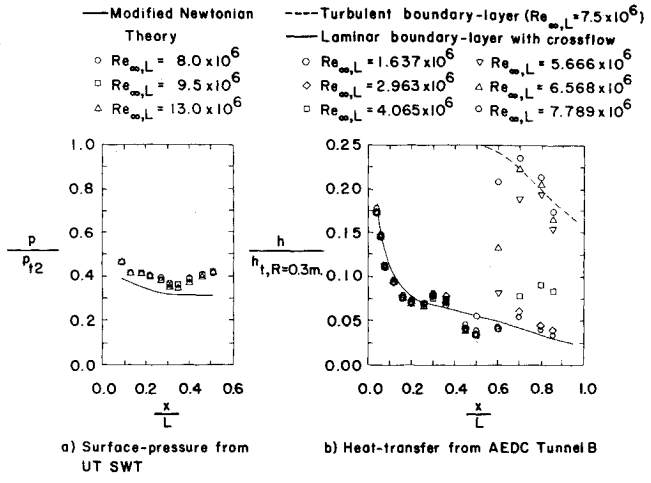

Fig. 3 Data from the windward pitch-plane of the UTN7 at a nominal alpha of 30°.

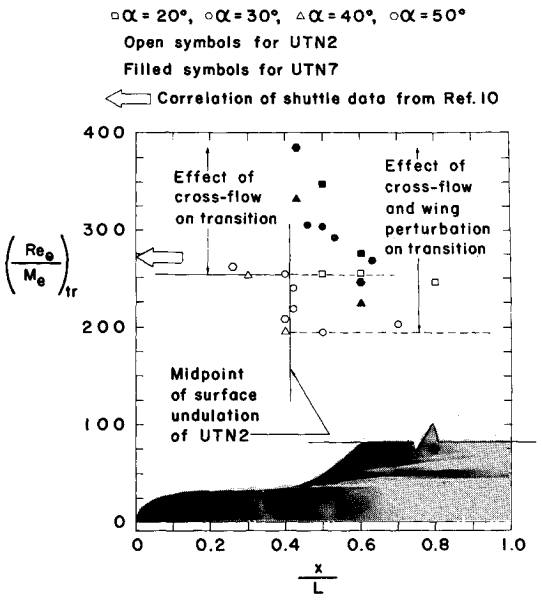

Fig. 5 Effects of nose bluntness and the fillet-induced perturbation on windward transition.

Discussion

Windward Flowfield

The surface-pressure and the heat-transfer distributions for the windward pitch-plane of the UTN7 and the UTN2 models are presented for an alpha of 30° in Figs. 3 and 4, respectively. The experimental pressure data are compared with the theoretical values calculated using modified Newtonian theory. The local heat-transfer coefficients have been divided by the theoretical[9] heat-transfer coefficient at the stagnation point of a 0.019-scale model sphere whose full-scale radius is 0.3m (i.e., 1.0 ft). The theoreticai heat-transfer distributions were calculated using the techniques described in Ref. 2.

The fillets formed by the complex, concave fairing in the wing-root region markedly affected the windward flowfield. The fillet-induced perturbation has the greatest effect on the data for the UTN7. A shock wave generated by the fillet causes a pressure rise downstream of $x = 0.3L$, which can be seen in Fig. 3. Furthermore, heat-transfer increases are evident at the thermocouples from $x = 0.3L$ to $x = 0.36L$ because of the shock : boundary-layer interaction. The subsequent decrease in heat transfer, which is evident at the thermocouples from $x = 0.425L$ to $x = 0.50L$, is attributed to the thickened boundary layer as the flow is funneled toward the plane-of-symmetry by the wing : fuselage flowfield interaction. Downstream of $x = 0.5L$, the experimental heat-transfer coefficients increase with Reynolds number. It is in this region that the heat transfer measurements become significantly greater than the theoretical distribution for a laminar boundary layer. Furthermore, the heat-transfer measurements for the highest Reynolds number are in good agreement with the theoretical values for a turbulent boundary layer. Thus, these heat-transfer data indicate the onset of boundary-layer transition.

Because of the relatively flat windward surface of the UTN2 nose, the fairing represents only a modest change in the cross sections (see Fig. 2). The sharply defined oil accumulation near $x = 0.34L$ (in Fig. 5) indicates that the extent of the fillet-perturbed flow is limited. A fillet-generated shock wave is evident in the flow-visualization photographs (e.g., Fig. 6, which depicts the UTN7 shock wave), yet neither the surface pressures nor the heat transfer for the UTN2 (Fig. 4) indicates a shock-induced increase or a subsequent decrease as the boundary-layer thickens (as were observed for the UTN7). A slight undulation of the model surface (which occurred during the run schedule) results in the relatively low heat-transfer coefficients measured

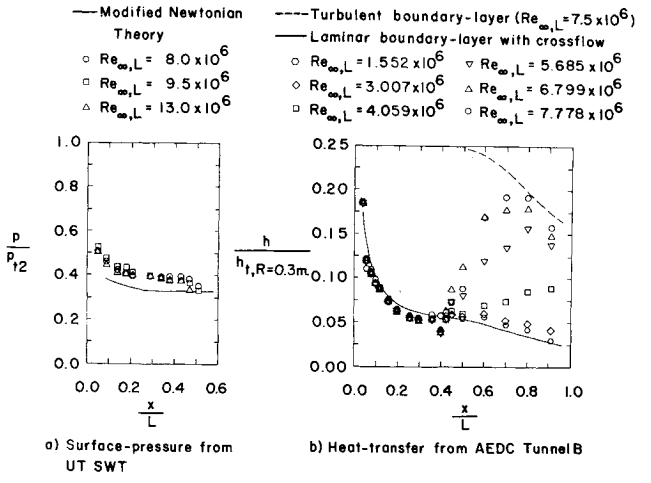

Fig. 4 Data from the windward pitch-plane of the UTN2 at a nominal alpha of 30°.

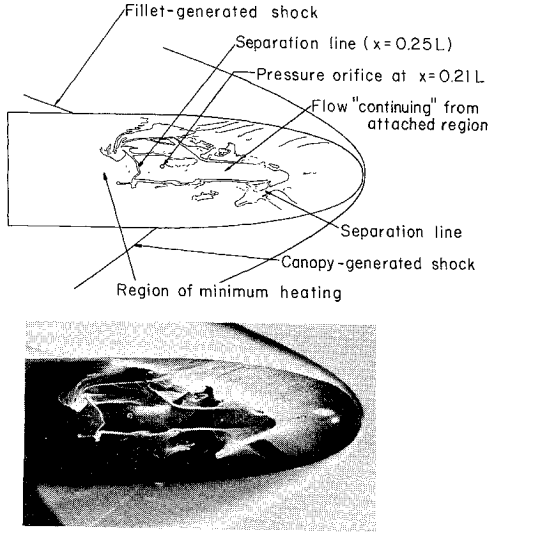

Fig. 6 Flow-visualization photograph and sketch showing leeward oil-flow patterns for the UTN7 at an alpha of 30°, $M_\infty = 4.97$.

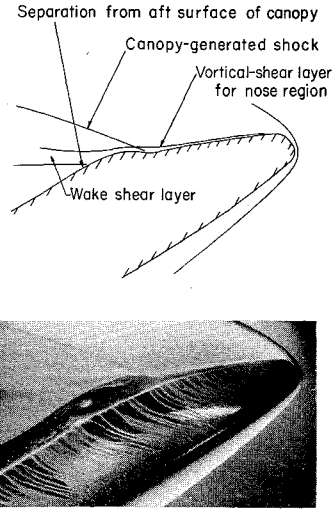

Fig. 7 Side-view flow-visualization photograph and sketch for the UTN2 at an alpha of 30, $M_\infty = 4.97$.

at $x = 0.4L$. Downstream of $x = 0.4L$, the heat-transfer data depend on Reynolds number, indicating the onset of transition. As noted below, the onset of transition appears to be affected by the undulation.

For the present investigation, the onset of boundary-layer transition was chosen to be the "point" where the heating rate deviated from the theoretical laminar distribution (see Figs. 3 and 4). The current results for the onset of boundary-layer transition are presented in Fig. 5 in terms of a parameter commonly used for shuttle entry-configurations, i.e., $(Re_\theta/M_e)_{tr}$. In a review of shuttle data, Scottoline[10] found that $(Re_\theta/M_e)_{tr} = 272$ was typical for shuttle entry-configurations. Transition sticking is evident for both configurations in the vicinity of wing-root fairing, or fillet. The oil-flow pattern (e.g., that for the UTN2 at an alpha of 35°, which is included in Fig. 5) shows a marked accumulation of oil where the fillet-generated shock crosses the nose. Thus, as one would expect, the fillet-shock: boundary-layer interaction tends to trip the boundary layer. Note that transition sticking for the UTN2 is most pronounced at $x = 0.41L$, which corresponds to the midpoint of the surface undulation. Thus, the UTN2 data reflect the effects both of the cross-sectional change and of the surface irregularity. For the UTN7, the transition-sticking phenomena is gradual and the values of $(Re_\theta/M_e)_{tr}$ approach 400. The impact of the fillet-shock induced perturbation on the transition criteria is strongly dependent on the upstream geometry of the windward fuselage. Furthermore, the geometry of the windward surface affects the transition parameters upstream of the wing juncture, i.e., $x < 0.4L$. The increased cross flow results in a significantly higher value of the transition parameter for the UTN7.

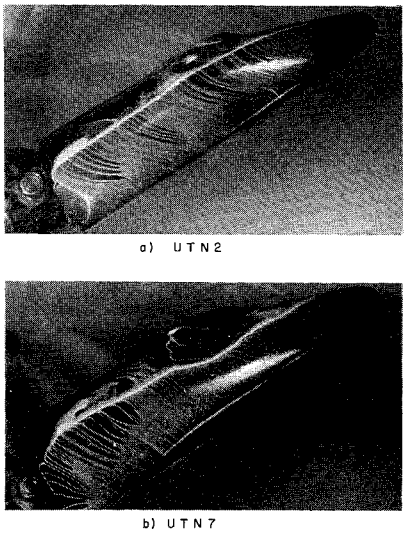

Fig. 8 Side-view oil-flow patterns for the UTN2 and for the UTN7 at an alpha of 30°, $M_\infty = 4.97$.

Leeward Flowfield

Flow visualization photographs

The lee-surface oil-flow pattern and the top-view schlieren for the UTN7 at an alpha of 30° are combined in Fig. 6. A sketch of the flowfield is included to help identify the various flow phenomena in the photograph. One can see both the fillet-generated shock wave (which produced the perturbations in heat transfer and in surface pressure evident in the windward data of Fig. 3) and the canopy-generated shock wave. The oil-flow pattern for the nose region at this angle of attack indicates a free-vortex type of separation, as described in the Introduction. The fact that a shearing force has removed the oil from the leeward plane-of-symmetry indicates a strong axial-flow component in this region. The accumulation of oil at $x = 0.25L$ indicates that this axial flow separates from the canopy surface. Oil flowing from the side of the canopy toward the low-pressure region just aft of the axial separation location leaves a spiral trace. Thus, the canopy breaks up the original separation pattern, creating a new vortical shear-layer.

The side-view schlieren photograph (Fig. 7) of the UTN2 at an alpha of 30° gives further evidence of the flow mechanisms described above. The free vortex type of separation appears as a relatively thick shear-layer ahead of the canopy. A shock wave is generated when the flow, which has a strong axial-flow component, encounters the windshield. The flow separation, which can be seen near $x = 0.25L$, is consistent with the oil-flow patterns.

Side-view oil-flow patterns are presented in Fig. 8 for both configurations. The accumulation of oil identifies the line along

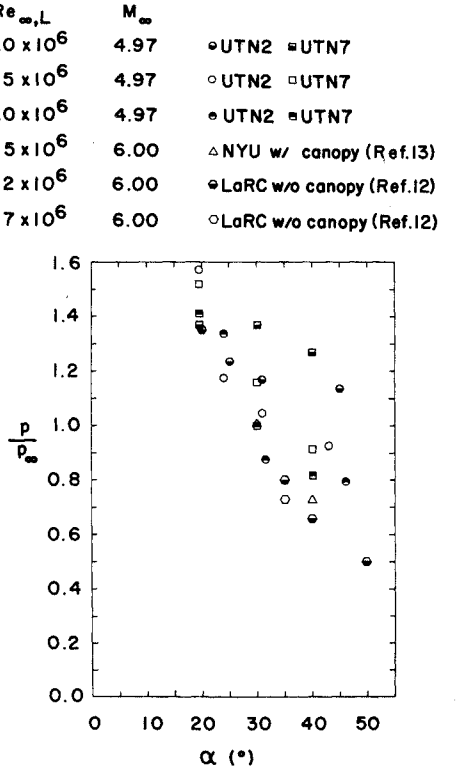

Fig. 9 Surface pressures measured at an orifice in the leeward pitch-plane, forward of the canopy.

which the "circumferential" component of shear vanishes. For the UTN2, the separation line closely follows the abrupt change in cross section (see Fig. 2). The canopy did not affect the separation contour of the UTN2 for any alpha tested, i.e., $20° \leqq \alpha \leqq 45°$. (The reader is referred to Ref. 11 for additional flow-visualization photographs.) However, the separation line shifts upstream in the vicinity of the canopy for the UTN7. Thus, the circumferential flow created by the elliptic cross sections of the UTN7 results in a strong interaction with the canopy-influenced flow. The canopy influence is most pronounced at an alpha of 20° and vanishes at a nominal alpha of 40°, where the separation lines for both configurations are similar.

Pressure and heat transfer

The effect of Reynolds number and of angle of attack on the leeward pressures is illustrated by the data of Fig. 9. Pressure measurements for the UTN2 and for the UTN7 are presented for an orifice located ahead of the canopy in the leeward pitch-plane ($x = 0.08L$). For angles of attack of 30° or greater, the leeward surface-pressures decreased as the Reynolds number increased (for the range of conditions tested). Since the leeward pressures were essentially independent of the Reynolds number at lower alphas, the Reynolds-number dependence is associated with flow separation. The relation between the leeward surface-pressure and the configuration geometry appears to depend on alpha. This is not surprising since the canopy-induced perturbation of the separation line for the UTN7 is a function of alpha.

Also presented in Fig. 9 are pressures[1,2,13] measured at similar locations on other orbiter-like configurations. Thus, in view of the pressure difference due to geometry for the UTN2 and for the UTN7 configurations, the agreement between the pressure measurements in this region is considered acceptable for the three tests. Only at the highest angle of attack are the current data significantly above the data of Ref. 12. The canopy-generated shock wave, which has been discussed, caused the relatively higher pressures. The configuration of Ref. 12 had no canopy.

The heat-transfer distributions for the leeward pitch-plane are presented in Fig. 10 for an alpha of 30°. This is the lowest angle of attack at which the canopy-generated flowfield perturbation causes the heat-transfer to increase at thermocouples upstream of the canopy. It is also the lowest angle of attack at which the surface pressures in this region exhibit the Reynolds-number dependence associated with flow separation. The characteristics of the heat-transfer distribution upstream of the canopy differ for the two configurations. For the UTN7, the heating perturbation is evident at only one thermocouple forward of the canopy and increases in magnitude with Reynolds number (as did the heat transfer on the windshield). The canopy-induced perturbation for the UTN2 extends further upstream but causes only a slight heating increase, which is essentially independent of Reynolds number. The peak heat-transfer, which occurred on the windshield, was significantly greater for the UTN2 than

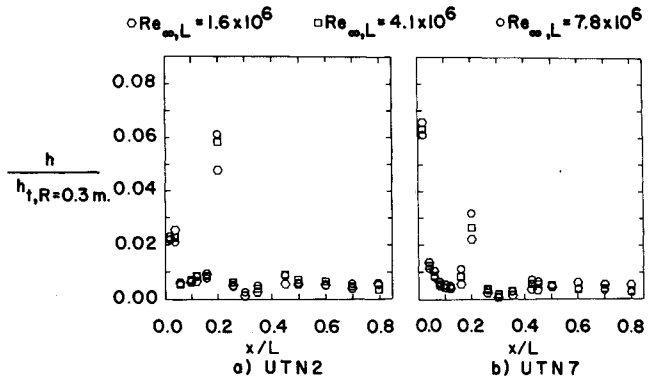

Fig. 10 The heat-transfer distribution for the leeward pitch-plane for the orbiters at an alpha of 30°.

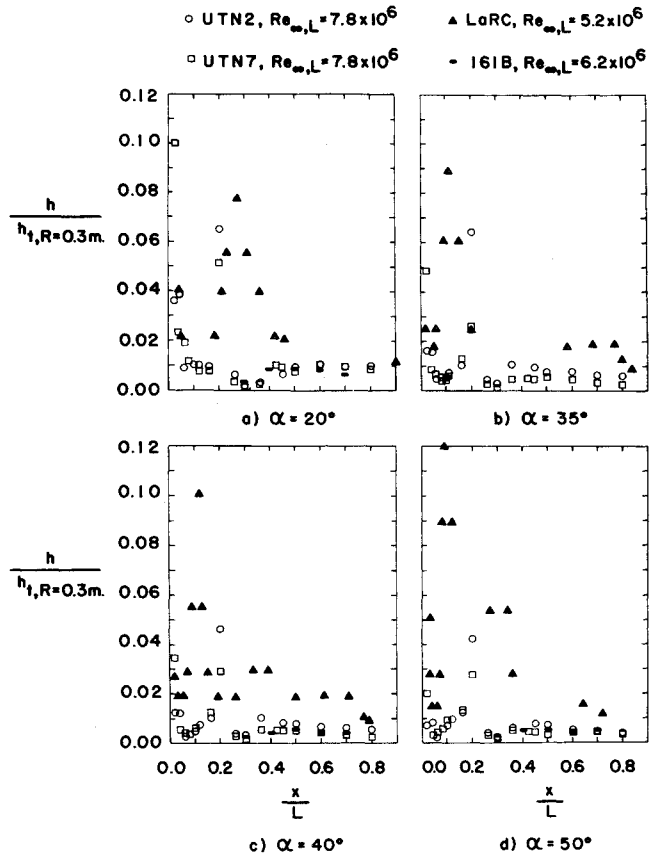

Fig. 11 A comparison of heat-transfer distributions in the leeward pitch-plane for delta-wing orbiters.

for the UTN7. The lower heat-transfer to the UTN7 is attributed to the convergence of the circumferential flow and of the leeward axial-flow (which has been noted previously and which results in a thicker shear layer). For both configurations, the minimum heat-transfer rate was measured at $x = 0.3L$, on the aft surface of the canopy. Further downstream, on the leeward surface of the fuselage, i.e., $x \geqq 0.4L$, the heat transfer exhibits only a weak dependence on Reynolds number or on the x-coordinate. However, the differences are relatively small and the heat-transfer in this region is relatively low for both configurations.

Heat-transfer distributions for the leeward pitch-plane are presented in Fig. 11 for both configurations for alphas from 20° to 50°. Also presented in Fig. 11 are the data obtained in the Langley 20-in., Mach 6 tunnel[12] for a delta-wing orbiter (which had no canopy) and the data obtained in Tunnel B[14] for the NAR 161B, a delta-wing orbiter with a canopy. The data were chosen so that the freestream conditions were roughly the same for all four configurations, i.e., comparable values of Mach number and of freestream Reynolds number based on model length. For a given angle of attack, the maximum heat-transfer measured on the configuration of Ref. 12 (using the phase-change-paint technique) is consistently higher than the peak value obtained in the present tests. (Note that it is possible to miss the peak value since only a finite number of thermocouples are available.) Of more significance is the fact that the heat-transfer downstream of the canopy location is consistently lower at all alphas for the present models. Furthermore, for the present configurations, the downstream heat-transfer is only weakly dependent on the x-coordinate (and on the Reynolds number), whereas a second heat-transfer peak is evident in this region of the model of Ref. 12 and increases in severity as alpha increases. The heat-transfer rates measured downstream of the canopy of the NAR 161B compare favorably with the present data. Thus, it appears that the presence of a protruding cockpit

changes the longitudinal component of flow and causes relatively low downstream heat-transfer.

Of the data from the leeward pitch-plane, the maximum heat-transfer and the maximum surface-pressure were always measured by sensors located on the canopy windshield. The peak heating rates and the peak pressures from the lee meridian are presented as a function of alpha in Figs. 12 and 13, respectively. For the UTN2, the peak lee-meridian pressure decreases continuously as alpha increases. The peak heating also decreases continuously with the alpha. For the UTN7, the peak lee-meridian pressure first decreased, then increased, with alpha. The peak lee-meridian, heat-transfer for the UTN7 also decreases with alpha up to an alpha of 30°. At higher angles of attack, the maximum leeward heating appears to be essentially independent of alpha. The change in slope at high angle of attack is consistent with the marked change in the canopy-region separation pattern observed in the oil flows, as described previously. The relation between alpha and the lee-meridian heating rates measured for the present configurations differed markedly from the correlation obtained in Ref. 12. The maximum heating rate measured in the leeward pitch-plane of the orbiter used in Ref. 12 increased as alpha increased. Furthermore, the location of the peak leeward heating was a function of the angle of attack for this configuration. For the present tests, the maximum heat-transfer rate always occurred at the thermocouples on the windshield.

The effect of configuration geometry on the relation between the peak values of surface pressure and of heat transfer should not be determined from the data of Figs. 12 and 13 because the instrumentation locations were not identical. Whereas the thermocouples for both the UTN2 and the UTN7 and the pressure orifice for the UTN7 were in the middle of the windshield, the pressure orifice for the UTN2 was near the base of the windshield. Since the pressure varied rapidly in this region, the mislocation, which was small on a physical scale (on the order of a millimeter), was significant.

General comments

The oil-flow patterns at an alpha of 30° indicate a free-vortex layer type of separation from the leeward surface upstream of the canopy for both configurations (see Fig. 6). A shock wave is generated when the vortical viscous flow encounters the canopy windshield, as can be seen in the side-view schlieren photographs (see Fig. 7). For alphas up to 30°, sudden and large increases in heat transfer and in surface pressure occur across the canopy-generated shock wave (see Fig. 11). Because the differences in nose geometry affect the three-dimensional character of the leeward flow at these alphas, the side-view

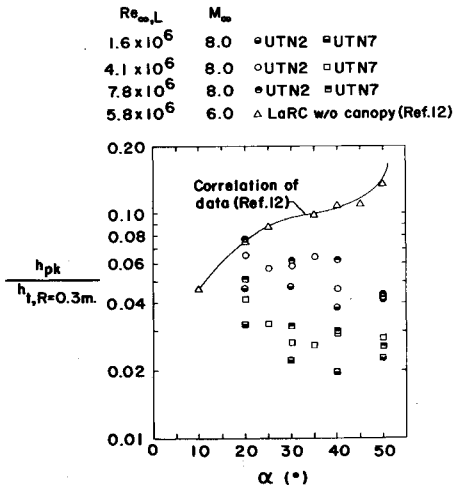

Fig. 12 Effect of angle of attack on the peak heat-transfer measurement in the leeward pitch-plane of delta-wing orbiters.

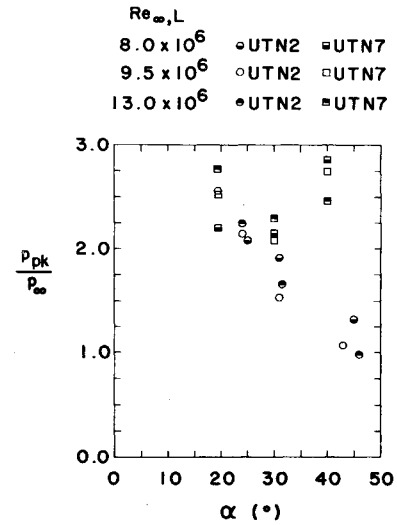

Fig. 13 Effect of angle of attack on the peak-surface pressure measurement in the leeward pitch-plane of delta-wing orbiters.

oil-flow patterns reflect the variations in the regions affected by the canopy-induced perturbations (see Fig. 8).

The canopy-induced flowfield perturbation extends well forward of the windshield at an alpha of 40°, as indicated by the increased heating beginning at $x = 0.06L$ in Fig. 11c. Although the schlieren photographs are not presented herein, a complex, canopy-generated shock wave is evident[11] for both configurations. At this high angle of attack, the pressure rise due to this shock feeds upstream, causing a secondary separation upstream of the canopy. The presence of a shock wave indicates a significant axial flow-component in the separated regions. The oil patterns for an alpha of 40° show that the side-surface streamlines are essentially perpendicular to the model axis and that the line along which the circumferential component of shear vanishes does not appear to be affected by the presence of the canopy for either configuration.

The oil-flow pattern of Fig. 6 and the trace of the viscous layer in the schlieren photograph of Fig. 7 indicate that the flow separates from the aft surface of the canopy at about $x = 0.25L$. As a result of this second separation, the heat-transfer and the surface pressure are a minimum on the aft surface of the canopy, i.e., at $x = 0.3L$ (see Fig. 10). Definitive flow-visualization photographs were not available for the leeward fuselage, i.e., aft of $x = 0.4L$. However, the heat-transfer in this region is relatively constant and low.

Conclusions

Based on the analysis of the data, the following conclusions are made for the configurations and test conditions of this program:

1) Local increases (which were configuration-dependent) in the heat-transfer and in the surface-pressure distributions occurred in the vicinity of the windward surface fairing which was required to mate the rounded nose to the flat underbelly of the windward fuselage.

2) The transition criteria were affected by cross flow in the nose region (i.e., nose bluntness). The carefully designed nose geometry eliminated transition-promoting inflection points in the bow shock, which together with cross flow yielded relatively high values of $(Re_\theta/M_e)_{tr}$ for the UTN7 model. The change in cross sections in the vicinity of the wing-root fairing produced a shock wave and transition sticking.

3) The flow visualization photographs indicate that the initial separation was of the free-vortex-layer type. Thus, there is a strong component of longitudinal flow which results in a canopy shock. The canopy shock was observed even at an alpha of

40°. The canopy-generated shock wave causes large local increases in heat-transfer and in surface pressure.

4) The flow visualization photographs and the uniformly low heating rates on the leeward fuselage indicate that the canopy serves to reduce the heating over a large area by breaking up the strong axial-flow component.

References

[1] Der. J., Jr., "A Study of General Three-Dimensional Boundary Layer Problems by an Exact Numerical Method," *AIAA Journal*, Vol. 9, No. 7, July 1971, pp. 1294–1302.

[2] Adams, J. C., Jr. and Martindale, W. R., "Hypersonic Lifting Body Windward Surface Flow-Field Analysis for High Angles of Incidence," AEDC, TR-73-2, Feb. 1973, Arnold Engineering Development Center, Tullahoma, Tenn.

[3] Wang, K. C., "Separation Patterns of Boundary Layer Over an Inclined Body of Revolution," *AIAA Journal*, Vol. 10, No. 8, Aug. 1972, pp. 1044–1050.

[4] Stetson, K. F., "Experimental Results of Laminar Boundary Layer Separation on a Slender Cone at Angle of Attack at $M_\infty = 14.2$," ARL 71-0127, Aug. 1971, Aerospace Research Labs., Wright-Patterson Air Force Base, Ohio.

[5] Hefner, J. N. and Whitehead, A. H., Jr., "Lee Side Investigation, Part I—Experimental Lee-Side Heating Studies on a Delta-Wing Orbiter," *NASA Space Shuttle Technology Conference, Vol. I—Aerothermodynamics, Configurations, and Flight Mechanics*, TM X-2272, April 1971, NASA.

[6] Hefner, J. N. and Whitehead, A. H., Jr., "Lee Side Flow Phenomena on Space Shuttle Configurations at Hypersonic Speeds, Part II—Studies of Lee-Surface Heating at Hypersonic Mach Numbers," *NASA Space Shuttle Aerothermodynamics Technology Conference, Vol. II—Heating*, TM X-2507, Feb. 1972, NASA.

[7] Young, C. H., Reda, D. C., and Roberge, A. M., "Hypersonic Transitional and Turbulent Flow Studies on a Lifting Entry Vehicle," *Journal of Spacecraft and Rockets*, Vol. 9, No. 12, Dec. 1972, pp. 883–888.

[8] Bertin, J. J., et al., "The Effect of Nose Geometry on the Aerothermodynamic Environment of Shuttle Entry Configurations," Aerospace Engineering Rept. 73001, Jan. 1973, The Univ. of Texas at Austin, Austin, Texas.

[9] Fay, J. A. and Riddell, F. R., "Theory of Stagnation Point Heat Transfer in Dissociated Air," *Journal of the Aeronautical Sciences*, Vol. 25, No. 2, Feb. 1959, pp. 73–85, 121.

[10] Scottoline, C. A., "Determination of Aerothermodynamic Uncertainties with Application to Space Shuttle Vehicles," *NASA Space Shuttle Aerothermodynamics Technology Conference, Vol. II—Heating*, TM S-2507, Feb. 1972, NASA.

[11] Bertin, J. J. and Faria, H. T., "Effect of Geometry on the Nose-Region Flowfield of Shuttle Entry-Configurations," Aerospace Engineering Rept. 73002, Aug. 1973, The Univ. of Texas at Austin, Austin, Texas.

[12] Hefner, J. N., "Lee-Surface Heating and Flow Phenomena on Space Shuttle Orbiters at Large Angles of Attack and Hypersonic Speeds," TN D-7088, Nov. 1972, NASA.

[13] Zakkay, V., Miyazawa, M., and DeSimone, G., "Reynolds Number and Mach Number Effect on Space Shuttle Configuration," Final Rept. NASA Grant NGR-33-016-129, Sept. 1972, New York University, Bronx, N.Y.

[14] Warmbrod, J. D., Martindale, W. R., and Mathews, R. K., "Heat Transfer Rate Measurements on North American Rockwell Orbiter (161B) at Nominal Mach Number of 8," DMS-DR-1177, Vol. III, Dec. 1971, Arnold Engineering Development Center, Tullahoma, Tenn.